

Article

Development of a Nanocrystal Formulation of a Low Melting Point API Following a Quality by Design Approach

Andreas Ouranidis ^{1,2,*}, Nikos Gkampelis ¹, Catherine Markopoulou ¹, Ioannis Nikolakakis ¹ 
and Kyriakos Kachrimanis ^{1,*} 

¹ Department of Pharmaceutical Technology, School of Pharmacy, Aristotle University of Thessaloniki, 54124 Thessaloniki, Greece; ngkampel@pharm.auth.gr (N.G.); plevend@gmx.com (C.M.); yannikos@pharm.auth.gr (I.N.)

² Department of Chemical Engineering, Aristotle University of Thessaloniki, 54124 Thessaloniki, Greece

* Correspondence: ouranidis@cheng.auth.gr (A.O.); kgk@pharm.auth.gr (K.K.); Tel.: +30-231-099-7666 (A.O.)

Abstract: Preparation of nanocrystal formulations by wet media milling and spray-drying is a reliable technique to enhance dissolution and ameliorate absorption limitations of poorly soluble BCS II drugs. However, when thermosensitive compositions are dried at high temperatures, the risks of particle aggregation and thermal degradation must be considered. The present study investigates the effects of nanosuspension formulation variables when performing the spray drying process at equidistant temperatures above and below the melting point. Towards this purpose, Fenofibrate is exploited as a model drug of unfavorable pharmacokinetic profile and low melting point (79–82 °C), properties that render thermal processing a nontrivial task. Rationalizing the system's behavior by combining molecular simulations with QbD methodology, the preparation of stable nanocrystals can be “steered” in order to avoid undesirable melting. The statistically resolved operational conditions showed that Fenofibrate Critical Quality Attribute-compliant nanosuspensions i.e., bearing hydrodynamic diameter and ζ -potential of 887 nm and -16.49 mV, respectively, were obtained by wet milling drug to Pharmacoat and mannitol weighted optimum ratios of 4.075% and 0.75%, after spray drying at the desired temperature of 77 °C. In conclusion, we present a quality assurance methodology of nano-comminution generally applicable for thermo-labile BCS II drugs.

Keywords: wet media milling; spray drying; nanocrystals; slip planes; energy frameworks; surface adsorption; stabilizer; solubility; Fenofibrate



Citation: Ouranidis, A.; Gkampelis, N.; Markopoulou, C.; Nikolakakis, I.; Kachrimanis, K. Development of a Nanocrystal Formulation of a Low Melting Point API Following a Quality by Design Approach. *Processes* **2021**, *9*, 954. <https://doi.org/10.3390/pr9060954>

Academic Editor:
Doraiswami Ramkrishna

Received: 17 May 2021
Accepted: 26 May 2021
Published: 27 May 2021

Publisher's Note: MDPI stays neutral with regard to jurisdictional claims in published maps and institutional affiliations.



Copyright: © 2021 by the authors. Licensee MDPI, Basel, Switzerland. This article is an open access article distributed under the terms and conditions of the Creative Commons Attribution (CC BY) license (<https://creativecommons.org/licenses/by/4.0/>).

1. Introduction

Fenofibrate (Figure 1) is a poorly soluble BCS class II active pharmaceutical ingredient (API), acting as a cholesterol lowering agent, administered per os either as monotherapy or in combination with statins for the treatment of hypercholesterolemia and hypertriglyceridemia [1]. Fenofibrate's mechanism of action relies on stimulating the peroxisome proliferator activated receptor- α (PPAR- α), which modulates the transcription of gene regulators of the cholesterol metabolism [1].



Figure 1. Fenofibrate chemical formula.

Fenofibrate's lipid-combating efficacy appears prone to the influence of non-fasted state conditions effecting a rather inconsistent and suboptimal pharmacokinetic profile.

In particular, numerous marketed products i.e., micronized capsules (Fenoglide[®]), microcoated micronized tablets (Lofibra[®]) and hard gelatin capsules (Lipofen[®]) require the presence of a high-fat meal in order to deliver satisfactory therapeutic absorption [2].

To avoid such dispensing limitations, novel Fenofibrate formulations have been developed that may also be administered free of companion meals, in the form of either nanoparticle tablets (Tricor[®], IDD-P tablets Triglide[®]) or micronized capsules (Antara[®]) [1]. The above refer to reduced size formulations promoting API enhanced solubility/dissolution profiles owing to increased particle surface area [3]. This iterated critical quality attribute (CQA) is met by particle nanonization wet media milling [4] processes, commonly performed by planetary ball mills [5,6]. The latter apply superimposed counter rotations between the mill jar and the grinding beads [7], generating shear stress, which in turn promotes crack propagation and fracture. The resulting nanocrystals possess high specific surface area, increasing the system's Gibbs surface free energy, rendering the system thermodynamically unstable. Owing to the nanosuspensions' thermodynamic instability, Ostwald ripening and agglomeration [8] take place, reversing the particle size reduction process.

These unwanted phenomena may be artificially hampered by the addition of non-ionic and/or ionic surfactants and polymeric agents known as nanosuspension stabilizers, which are adsorbed by the particle surfaces and prevent agglomeration by electrostatic and/or steric hindrance. Several additives such as PVA, PVP, polysorbates, Poloxamers, Solutol, stabilize the crystal face [9] although also promoting the "adsorption induced reduction of solid strength", AIRS, known as the Reh binder effect [10]. Despite the substantial kinetic stabilization achieved by the addition of polymeric additives, nanosuspensions eventually undergo quality deterioration owing to sedimentation, agglomeration and/or Ostwald ripening. Therefore, drying processes are employed to establish the material's thermodynamic stability and further processability. During spray drying, nanosuspensions are atomized first to single droplets and are then immediately dried on heated gas streams. Although atomization increases the surface area available for heat transfer, the suitable operating inlet temperature [11] must be imposed to facilitate the evaporation of the liquid phase. This may become an important issue when drying needs to be performed at a temperature range that approximates the melting point of the nanocrystalline material, increasing the risk of particle aggregation or thermal degradation. In addition, during the high energy mixing with excipients, eutectic compositions may occur, further inducing melting point depression.

Fenofibrate exhibits low melting point (81 °C) while higher temperatures have been implemented according to the literature, in order to evaporate the moisture content by spray drying [12,13], i.e., increasing the risk of nanocrystal agglomeration and thermal degradation [14]. Nevertheless, attempts of improving Fenofibrate's dissolution and bioavailability profile by a combination of milling and spray drying are ongoing. The conversion of several aqueous dispersion mixtures of nanolipid carriers processed to dry powder by spray drying at 100 °C has been described as a workable approach to achieve improved physical-chemical stability compared to the aqueous dispersion [15]. Global Pharmaceutical development Merck investigated the effects of co-grinding with follow up of spray-drying at 150 °C, as powerful techniques for the preparation of rapidly dissolving fenofibrate formulations, that lead to bioavailability improvements of oral fenofibrate products [16]. The iterated approaches employed inlet processing temperatures above the melting point of the API, undertaking the relevant risks.

However, none of the published works have investigated the effects of the process parameters and formulation variables on Fenofibrate's nanosuspensions' critical quality attributes such as crystal size and mixture component stability, when spray drying is performed near the melting point. Therefore, the present study attempts to elucidate the effects that the milling process and nanosuspension formulation variables have on the particle size and ζ -potential of the material system, in the case scenario when the spray drying process is performed at equidistant inlet temperatures above and below

the API melting point. Through this work frame of process implementation, we attempt to specify the desirable design space, quantifying the contribution of the additives and excipients, while maintaining compliance to the Pharmacopeia ruling. We demonstrate both the strengths and limitations of our DoE approach, proposing a Quality Assurance (QA) supplementary method that should be installed to verify the standards of material properties of low melting point pharmaceutical substances.

2. Materials and Methods

2.1. Materials

Fenofibrate (Boots, London, UK) was kindly donated by VIANEX S.A. (Athens, Greece). Low viscosity grade HPMC (Pharmacoat 603) kindly donated by Shin-Etsu Chemical Co., Ltd., Japan, was used as suspension stabilizer. Mannitol (Pearlitol® 160C) kindly donated by Roquette Frères, (Lestrem, France) was used as co-milling agent, and dispersibility-enhancing spray drying diluent (matrix former). During wet milling, distilled water was used as the suspension medium.

2.2. Methods

2.2.1. Wet Media Milling

Wet media milling of Fenofibrate was performed on a laboratory planetary ball mill (Pulverisette 7 Premium, Fritsch GmbH, Germany) using 1 g of API, 70 g of ZrO₂ milling beads and three different drug–stabilizer (10:1, 5.5:1, and 2:1 *w/w*) and drug–mannitol ratios (2:1, 1:1, and 0.5:1 *w/w*). The API and additives were dispersed in 10 mL of distilled water and added into a 45 mL milling jar. Milling was performed at 450 rpm for 20 cycles of 3 min with 5 min interval breaks to prevent sample heating.

2.2.2. ATR-FTIR Spectroscopy

A sample of the powder was tested using an IR-Prestige-21 FT-IR spectrometer (Shimadzu Corporation, Kyoto, Japan) at the range of 600–4000 cm⁻¹ with resolution level 4 cm⁻¹ set at 32 scans per spectrum, averaged for each of investigated samples. The instrument was attached to a Golden-Gate MKII single reflection ATR (Specac, Kent, UK) equipped with ZnSe lenses of proper background subtraction. The FTIR spectra of the unprocessed physical mixtures were compared to the dried nanocrystalline product.

2.2.3. Particle Size and Polydispersity Index (PDI) Determination by Dynamic Light Scattering (DLS)

Samples of the nanosuspension were removed from the milling jar at 3, 6, 9, 15, 30 and 60 min in order to determine the particle size time evolution during milling. The particle size (Z-average, nm) and the polydispersity index (PDI) were determined by dynamic light scattering on a Zetasizer nano ZS instrument (Malvern Instruments, Cambridge, UK), after dilution to saline water. Material containing particle sizes outside of the DLS operating range, was additionally measured by optical microscopy. A sampled amount of nanosuspension was dispersed in drops of silicone oil on a slide, in order to determine the diameter length on a Laborlux S microscope (Leitz, Wetzlar, Germany), connected to a PC, following an automatic image analysis method with the Quantimet 500 software (Leica, Cambridge, UK).

2.2.4. Solidification of Nanosuspensions by SD

The resulting preparations of the nano-suspension by the milling process, were then inserted to a Mini Spray dryer, Büchi B-191 (Büchi, Flawil, Switzerland). After preliminary testing, the spray drying air flow rate was kept to 800 m³/h, aspirator to 80% and the pump speed to 5%. The effect of drying temperature was investigated relatively to the API melting point. Specifically, the drying process was carried out at the inlet operating temperatures of 71 and 91 °C, i.e., ±12% above and below the API melting temperature

(81 °C), respectively. For further analysis, the SD samples were preserved in a desiccator over phosphorus pentoxide.

2.2.5. Differential Scanning Calorimetry (DSC)

DSC measurements were performed on a heat-flux DSC 204 F1 Phoenix differential scanning calorimeter produced by NETZSCH (Selb, Germany). Weighted samples in the amounts of 3–5 mg were placed in pans of perforated aluminum and then scanned at temperature range between 40 °C and 90 °C at the heating rate of 10 °C/min. DSC measurements were applied on sample mixtures of drug with Pharmacoat 603 prepared by solvent drop grinding. In order to clarify the potential effects of stabilizer on the material's melting behavior, the measurements were compared to the unprocessed physical mixture (control) in terms of melting point depression. Accurately weighted amounts (5 mg ± 0.2 mg) of the sample were placed in aluminum pans. The DSC scans were performed for the temperatures between 25 and 100 °C at the same heating rate of 10 °C/min, under nitrogen flow of 50 mL/min.

2.2.6. Determination of Redispersibility

Each dried sample was estimated for its redispersibility. Approximately 2–3 mg were dispersed in 4 mL of distilled water and then sonicated for 20 s. The particle size was determined by DLS and whereas required (depending on the obtained size range) by optical microscopy using a PriorLux Pol microscope (Prior, Cambridge, UK). The redispersibility index, RDI, was calculated for each run according to [17], by the following equation:

$$\text{RDI} = \frac{D_0}{D}$$

where D_0 and D are the Z-average diameter of particles after milling before spray drying and after redispersion, respectively. The values of RDI approaching unity pinpoint that the nanosuspension regains the original particle size when dispersed in an aqueous medium.

2.2.7. Molecular and Solid-State Modeling

Solid state computer modeling offers invaluable insights on the arrangement in space of both organic [18] and inorganic material [19]. In this study the initial crystal coordinates of fenofibrate form I were taken from the Cambridge Crystallographic Database [20] (CSD Ref Code TADLIU01), in order to provide insight into the structural properties that in turn define the macroscopic mechanical and surface adsorption behavior of the drug's formulation with the stabilizer.

Crystal Morphology Modelling

The Bravais–Friedel–Donnay–Harker (BFDH) methodology was exploited to construct morphology models using the GDIS program [21] in order to identify the crystal surfaces that are more likely to exist. The resulting crystal faces were used to compute the attachment energy that defines the crystal growth morphology. Calculations for this scope were performed by the General Utility Lattice Program, GULP v.5.2 [22], employing the Dreiding 2.21 force field parameters [23] and atomic point charges derived from the CHELPG electrostatic potential at the 6-31G**/MP2 level of theory. The Firefly quantum chemistry package was used which is based on the GAMESS US [24] source code (Alex A. Granovsky, Firefly version 8.2, 5/2021, <http://classic.chem.msu.su/gran/firefly/index.html>, accessed on 1 May 2021).

Lattice Energy Frameworks

Fenofibrate's intermolecular forces in the crystal lattice were analyzed by the semiclassical density sums approach (SCDS-pixel) [19]. This method allows for the quantitative assessment of lattice pairwise interactions, yielding interaction energy components, namely coulombic, polarization, dispersion and repulsion. The electron density was calculated at

the 6-31G**/MP2 level of theory using the Firefly quantum chemistry package, and the pairwise interactions were calculated by the clp software (<http://www.angelogavezzotti.it>, accessed on 1 May 2021). The intermolecular interactions were visualized by building the Energy Vector Diagrams [25] with the help of the process Pixel package [26], and projected on the BFDH crystal morphology, using the Mercury software program [27].

2.2.8. Optimization of Wet Media Milling by Statistical Design of Experiment (DoE)

The amount of Fenofibrate was kept constant at 1 gr, Pharmacoat 603 was added as stabilizer and mannitol as a co-milling agent. The wet milling process totaled the duration period of 60 min, which was split in 20 grinding cycles of 3 min each followed by 5-min breaks. A rotation speed of 450 rpm was set, alternating the rotation direction after each milling cycle for 70 g of beads featuring 0.5 mm diameter. In order to evaluate the progression of the API's comminution, samples were withdrawn after 3, 6, 9, 15, 30, 45 and 60 min. The experimental design (DoE) of wet media milling and spray drying in order to optimize the procedure is shown by Table 1.

Table 1. DoE for the wet media milling and spray drying of Fenofibrate (FEN), using Pharmacoat 603 (HPMC) as stabilizer agent and mannitol as a co-milling agent.

| Std | Run | Factor A FEN/HPMC (w/w) | Factor B FEN/Mannitol (w/w) | Factor C Inlet Temperature (°C) |
|-----|-----|-------------------------------|-----------------------------------|---------------------------------------|
| 8 | 1 | 5.5 | 2 | $0.88 \times T_m$ |
| 1 | 2 | 2 | 0.5 | $0.88 \times T_m$ |
| 5 | 3 | 5.5 | 1 | $0.88 \times T_m$ |
| 4 | 4 | 2 | 1 | $0.88 \times T_m$ |
| 3 | 5 | 10 | 0.5 | $0.88 \times T_m$ |
| 18 | 6 | 10 | 2 | $1.12 \times T_m$ |
| 7 | 7 | 2 | 2 | $0.88 \times T_m$ |
| 16 | 8 | 2 | 2 | $1.12 \times T_m$ |
| 17 | 9 | 5.5 | 2 | $1.12 \times T_m$ |
| 2 | 10 | 5.5 | 0.5 | $0.88 \times T_m$ |
| 12 | 11 | 10 | 0.5 | $1.12 \times T_m$ |
| 13 | 12 | 2 | 1 | $1.12 \times T_m$ |
| 10 | 13 | 2 | 0.5 | $1.12 \times T_m$ |
| 14 | 14 | 5.5 | 1 | $1.12 \times T_m$ |
| 15 | 15 | 10 | 1 | $1.12 \times T_m$ |
| 9 | 16 | 10 | 2 | $0.88 \times T_m$ |
| 6 | 17 | 10 | 1 | $0.88 \times T_m$ |
| 11 | 18 | 5.5 | 0.5 | $1.12 \times T_m$ |

The factorial elements of A were set to facilitate three discrete drug to stabilizer ratio levels, namely 2:1 *w/w* (+, high quantity of HPMC), 5.5:1 *w/w* (0, medium quantity of HPMC), 10:1 (−, low quantity of HPMC). The factorial elements of B investigated three drug to mannitol ratio levels, namely 2:1 *w/w* (+, high quantity of mannitol), 1:1 *w/w* (0, medium quantity of mannitol), and 0.5:1 *w/w* (−, low quantity of mannitol). The resulting nanosuspensions were immediately spray dried as prepared, at inlet temperatures of $0.88 \times T_m$ and $1.12 \times T_m$, which roughly correspond to 71 and 90 °C (the T_m of fenofibrate was taken as 81 °C).

In total, 18 runs were conducted in order to examine the main effects and interactions of the iterated critical process parameters (drug–stabilizer ratio, drug–mannitol ratio and SD inlet temperature) on the final product material properties. The PQAs considered in this study were the Z-average diameter, the ζ -potential, and the redispersibility of the solidified agglomerates. Referring to the Z-average particle size and ζ -potential, the standard least squares method of multiple linear regression was employed to model the data by calculating the respective factorial probability values (*p*-values). ANOVA was applied to infer supplementary cause and effect relationships, i.e., the factors classify

the data points into one of the groups causing the mean value difference. Numerical optimization was used to determinate the desired operating space. Moreover, three-dimensional surface plots were annotated to visualize the CQA responses relative to the two-factor interactions.

3. Results and Discussion

3.1. Wet Media Milling

Diluent/Co-Milling Agent

Pharmacoat 603 mixed with mannitol 1:1 *w/w* were ATR-FTIR tested to compare the spectra of their dried mixtures for observing possible intermolecular interactions (Figure 2) before and after spray drying. In detail, shift peaks at 3350 and 3000 cm^{-1} were attributed to the vibrations of the C-H and of O-H bonds, respectively. Mannitol was preferred as the suitable diluent, hence was deemed more likely to interact with Pharmacoat-603 explaining the high observed reflectance levels illustrated by Figure 2. The spectra verified that spray drying the commercial form of the API did not produce any identifiable polymorphic elements.

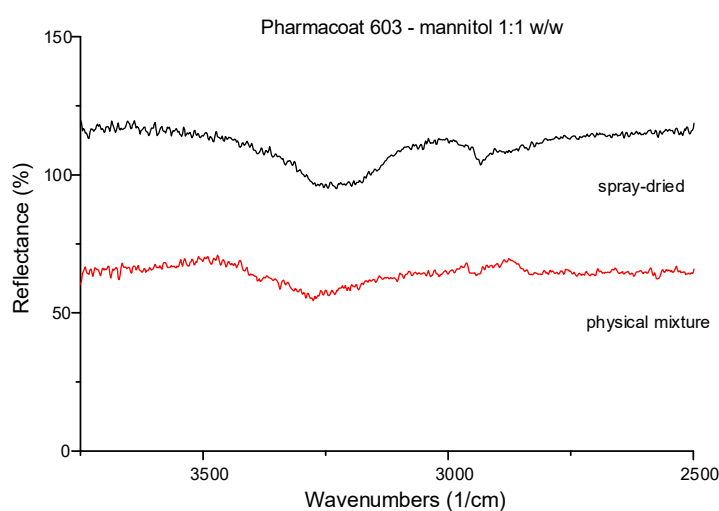


Figure 2. Representative ATR-FTIR spectra of 1:1 *w/w* physical mixture of Pharmacoat 603 with mannitol before and after spray-drying.

3.2. Wet Media Milling Process Optimization

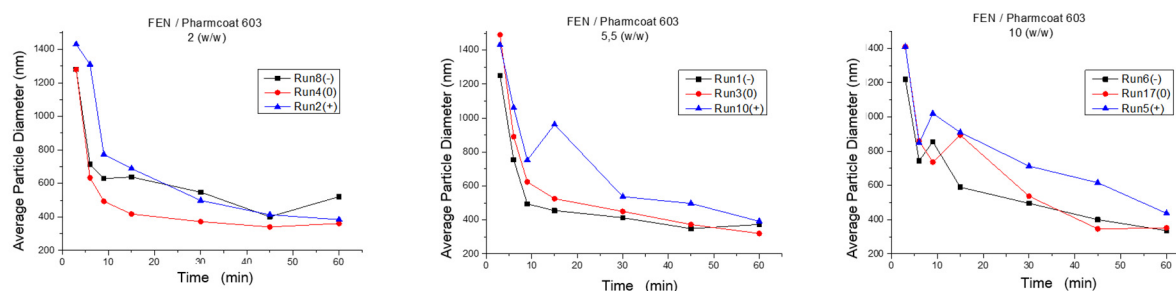
3.2.1. Effects of Stabilizer and Mannitol Ratio on Fenofibrate Particle Size

Table 2 lists the results of Fenofibrate's particle size obtained post the wet media milling process completion. The optimal milling time interval found to achieve the finest crystal size was between 45 and 60 min. Concerning the cases of Runs 1 and 9, 7 and 8, 4 and 12, and 15 and 17 pertaining to mannitol mixture participation range from medium to low DoE levels, the hydrodynamic crystal diameter appears to not further decrease after enduring 45 min of milling, but instead particles rather tend to aggregate.

Table 2. Z-Average size diameter of Fenofibrate during milling with Pharmacoat 603, according to the experimental design.

| Time (min) | Z-Average (nm)/Run Number | | | | | | | | |
|------------|---------------------------|-----------|----------|---------|----------|-----------|---------|----------|----------|
| | 6 and 16 | 15 and 17 | 5 and 11 | 1 and 9 | 3 and 14 | 10 and 18 | 8 and 7 | 4 and 12 | 2 and 13 |
| 3 | 1220 | 1410 | 1410 | 1250 | 1490 | 1430 | 1280 | 1280 | 1430 |
| 6 | 744 | 860 | 848 | 754 | 890 | 1060 | 713 | 633 | 1310 |
| 9 | 855 | 736 | 1020 | 494 | 624 | 752 | 629 | 493 | 773 |
| 15 | 590 | 894 | 910 | 455 | 525 | 962 | 638 | 417 | 689 |
| 30 | 495 | 537 | 713 | 413 | 450 | 537 | 548 | 372 | 498 |
| 45 | 400 | 346 | 616 | 349 | 373 | 497 | 401 | 340 | 413 |
| 60 | 336 | 352 | 473 | 373 | 320 | 392 | 521 | 361 | 384 |

Moreover, high mannitol content represented by Runs (5 and 11, 10 and 18, 2 and 13) generally seems to contribute to lower grinding effectiveness, resulting in nanocrystals of larger particle size. Specifically, as illustrated by Figure 3, the most suitable numeric region of mixture composition among the experimental range of the wet media milling being considered as a standalone block unit, was obtained by the Runs 3 and 14, where the ratio of drug to stabilizer was 5.5 *w/w* and the drug to mannitol ratio was 1:1 *w/w*. Results combining acceptable CQAs and low stabilizer quantity were obtained by the Runs 15 and 17, and 6 and 16, whereas the drug to mannitol ratio was 1:1 *w/w* and 2:1 *w/w*, respectively.

**Figure 3.** Z-Average diameter of FEN's particle size during wet media milling as function of time: (+) FEN/mannitol 0.5 *w/w*, (0) FEN/mannitol 1 *w/w*, (−) FEN/mannitol 2 *w/w*.

Regarding the ζ -potential absolute values of Fenofibrate nanocrystals determined after 60 min of milling (Table 3), Runs 1 and 9, 5 and 11 and 6 and 16 were found lower than 20 mV, while all other Runs exhibit ζ -potential absolute values over 20 mV. The lower ζ -potential values are associated with low and medium stabilizer concentrations, whether in the case of Runs 1 and 9, with low diluent concentration.

Table 3. ζ -potential values of FEN nanocrystals in the presence of Pharmacoat 603, after 60 min of milling.

| Run Number | Z-Potential (mV) |
|------------|------------------|
| 1–9 | −13.2 |
| 17–15 | −22.8 |
| 4–12 | −25.6 |
| 2–13 | −24.0 |
| 10–18 | −24.6 |
| 8–7 | −23.8 |
| 3–14 | −26.4 |
| 5–11 | −18.6 |
| 6–16 | −15.4 |

3.2.2. Solidification and Redispersion of FEN Nanosuspension

The DSC analysis of Fenofibrate test samples coated with Pharmacoat 603 for 2.2 *w/w* and 1.2 *w/w* ingredient contribution, revealed distinct melting point depression when compared to the physical mixture curve displayed in Figure 4 as Initial FEN (melting onset temperature 75 vs. 80 °C, respectively). This interaction was taken into account when designing, setting up and optimizing the thermal process.

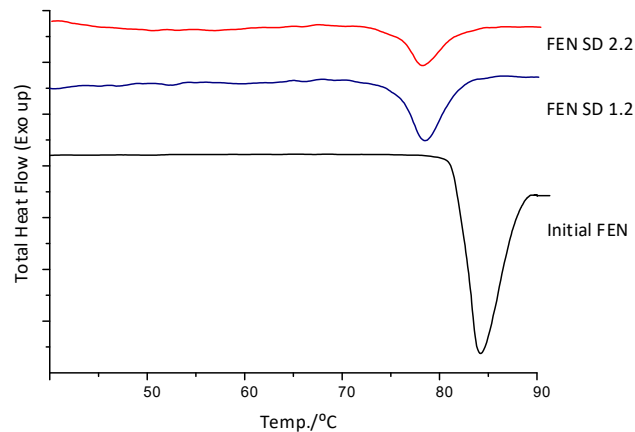


Figure 4. DSC diagrams of initial FEN and samples coated with Pharmacoat 603.

Correspondingly, after having quantified the melting point depression tendency of the working mixture, the spray drying process was implemented for two inlet operating temperatures at 71 and 91 °C, in agreement with the experimental design (Table 1). The dried material redispersibility properties were subsequently tested, and the results are listed in Table 4.

Table 4. Particle size, redispersibility index and ζ -potential of FEN before and after drying.

| Spray Dried at $0.90 \times T_m$ (71 °C) | | | | Spray Dried at $1.12 \times T_m$ (91 °C) | | | |
|--|----------------|---------|-------------------------|--|----------------|---------|-------------------------|
| Run | Z-Average (nm) | RDI (%) | ζ -Potential (mV) | Run | Z-Average (nm) | RDI (%) | ζ -Potential (mV) |
| 1 | 321 | 86.05 | −20.2 | 9 | 10,100 * | 2707 | −11.1 |
| 16 | 311 | 92.55 | −20.1 | 6 | 10,130 * | 3014 | −18.4 |
| 17 | 356 | 101.13 | −20.4 | 15 | 13,140 * | 3732 | −20.2 |
| 3 | 550 | 171.87 | −18.6 | 14 | 644 | 201.2 | −14.8 |
| 5 | 425 | 97.25 | −19.8 | 11 | 13,410 * | 3068 | −19.8 |
| 7 | 377 | 72.36 | −19 | 8 | 521 | 100 | −14.8 |
| 10 | 305 | 77.80 | −16.4 | 18 | 694 | 177 | −16.8 |
| 2 | 432 | 112.5 | −13.8 | 13 | 730 | 190.1 | −17.2 |
| 4 | 370 | 102.49 | −16.4 | 12 | 441 | 122.2 | −15.2 |

* Size values were determined by optical microscopy.

Run 3 (drug–stabilizer ratio 5.5:1, drug–diluent ratio 1:1) shows an extreme RDI % reading of 171.87%, probably due to instrument or operator handling error, and was therefore excluded from the analysis. For the remaining Runs, when drying was performed below the melting point of the mixture, the processed nanosuspensions recovered their original Z-average size to a great extent, as indicated by their dispersibility index (RDI%), which varied from 86.05% to 112.5%. On the contrary, when the inlet drying temperature rises above the melting point threshold, the agglomeration effect ascends (Singh and den Mooter, 2016) resulting in particle size increase. Specifically, in the case of Runs 9, 6, 11, 14 and 15 the size increased outside of the instrument’s operating range and therefore it was advised to revert to optical microscopy, for the evaluation of the particle size diameter.

Regarding the ζ -potential absolute value, this was found higher in almost all Runs, when drying was performed below the melting point threshold, with the exception of Runs 2 and 13 where the stabilizer ratio was lowest. In the case of Runs 5 and 11 and 15 and 17 where the drug to stabilizer ratio was high, the ζ -potential remained unchanged implying that either no particle melting occurred that could cause particle agglomeration, or even if it did, the available quantity of stabilizer prevented contact and agglomeration of the individual molten particles, in the given mixture composition for both temperature levels. On the other hand, when spray drying is performed above the melting point, the stability of the mixture deteriorates. Runs 6 and 16 and 3 and 14, corresponding to drug:stabilizer ratio of 10:1 and 5.5:1 *w/w*, respectively, showed a ζ -potential increase. Nevertheless, in the first case the particle size formation was still valued outside of the desired PQA scale. Principally, as shown in Figure 5, for equal drug to stabilizer ratio the observed value of ζ -potential after spray drying, demonstrated a trend of the same range.

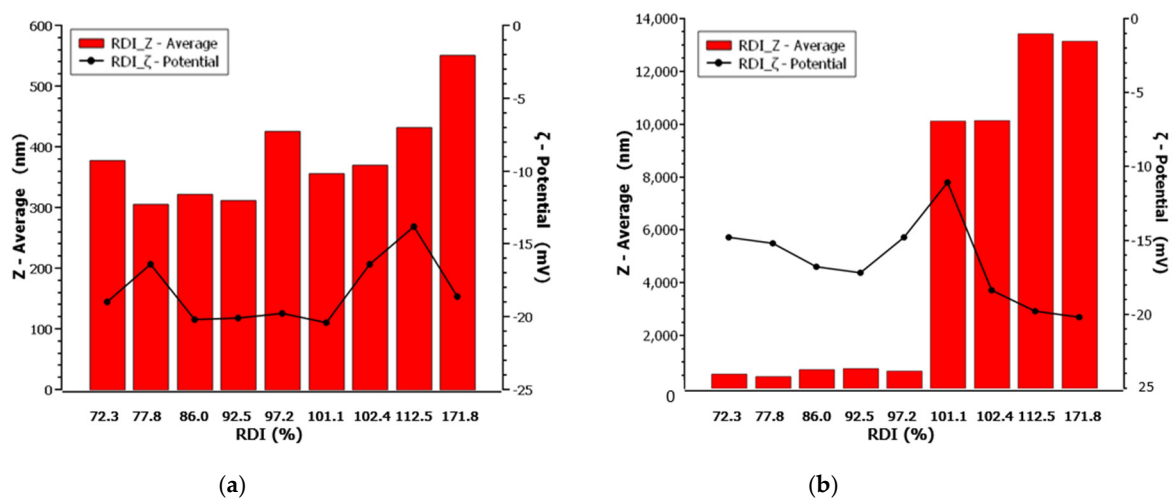


Figure 5. Particle size, redispersion index, and ζ -potential of FEN pre- and post-drying, respectively, at (a) 71 °C (below the melting point) and (b) 90 °C (above the melting point) of Fenofibrate.

For the rest of the Runs the ζ -potential absolute value became higher when drying was performed at 71 °C than at 91 °C. As expected, and in relation to the raw material, ζ -potential was reduced having endured the burdening, thermal process, associated effects on the system's stability [28]. Furthermore, ζ -potential appeared to exhibit dependence on the mannitol content, as demonstrated by the ATR-FTIR reduction of intensity owing to the dipole moment of recrystallizing above the melting point, as well as peak displacements at 3200 cm^{-1} correlated to C-H and O-H stretching vibrations.

According to the repeatable FTIR spectra presented in Figure 6, fenofibrate retains its crystal form (polymorph I, [29]) concisely, hence no polymorphic transformation was induced by the spray drying process at 91 °C inlet temperature.

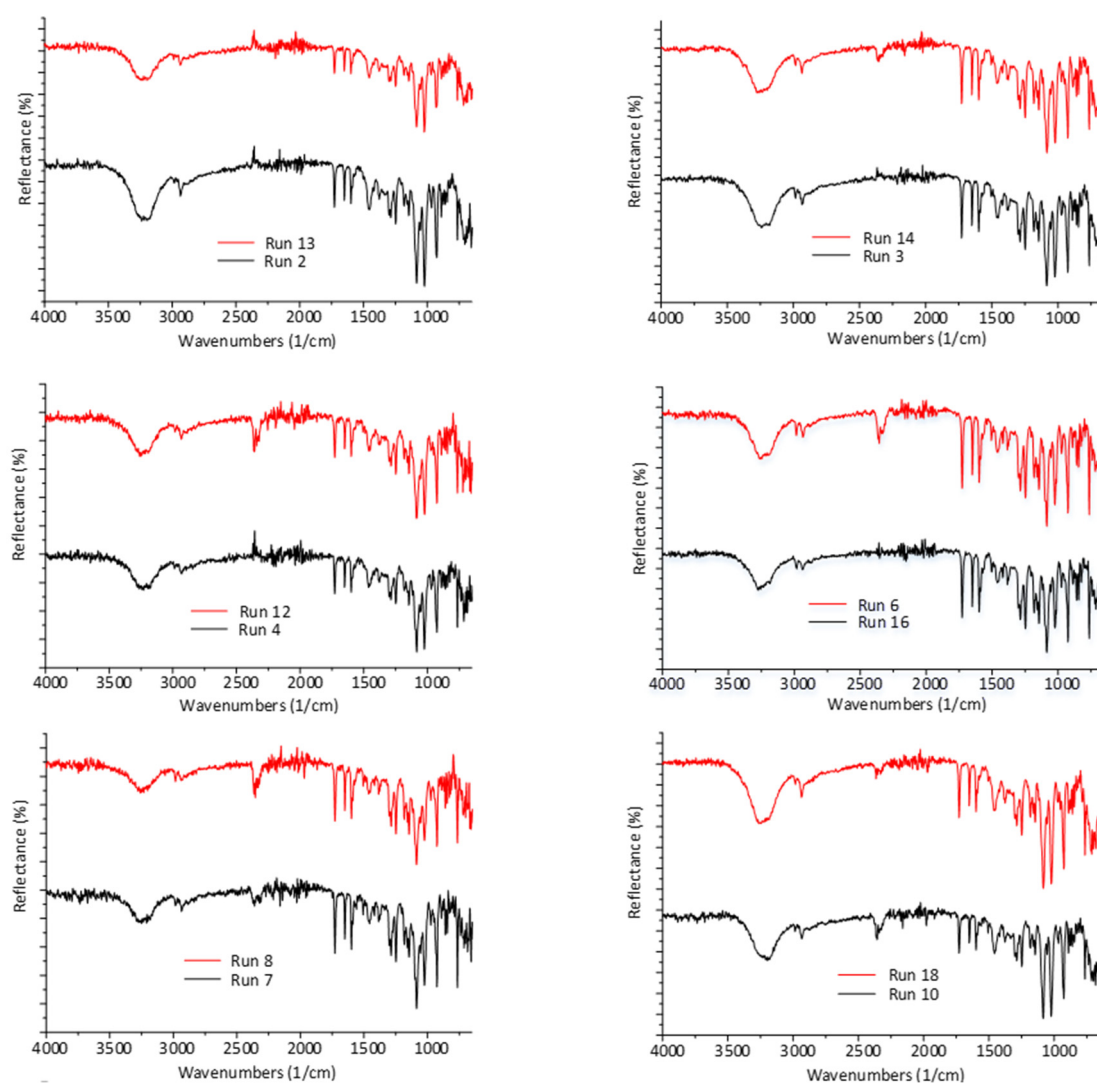


Figure 6. FTIR spectra of spray dried batches of the DoE, at inlet temperatures above (red) and below (black) the melting point of FEN.

3.3. Crystal Structure and Morphology

Figure 7 depicts a model of Fenofibrate commercial polymorph's crystal structure and morphology. The fracture mechanism of fenofibrate in the molecular–crystal level is proposed by the diagrams of the force vectors from SCDS–pixel interactions, alongside with the crystal morphology as calculated by the BFDH method (Bravais–Friedel–Donnay Harker) [30]. According to the SCDS–pixel method, the total energy of the crystal lattice is -139.7 kJ/mol, which is partitioned to individual energy components, namely dispersion -184.2 kJ/mol, repulsion 120.1 kJ/mol, electrostatic (Coulombic) -52.5 kJ/mol and polarization component of -23.2 kJ/mol. The dispersion interactions play a dominant role in stabilizing the crystal lattice, aided secondarily by the electrostatic and polarization components, as expected for a molecule that lacks hydrogen bond donor groups. The vectors of the dispersion and repulsive interactions were found to be overlapping, thus weakening the total stabilizing interaction in the specific direction. Based on these distributions of interactions, no preferred slip directions in the crystal lattice can be safely defined. However, the spatial distribution of intermolecular interactions explains why Fenofibrate, an apparently “soft” material of high compressibility, is in practice susceptible to brittle fracture, a finding that was verified by our experimental results (see Table 2).

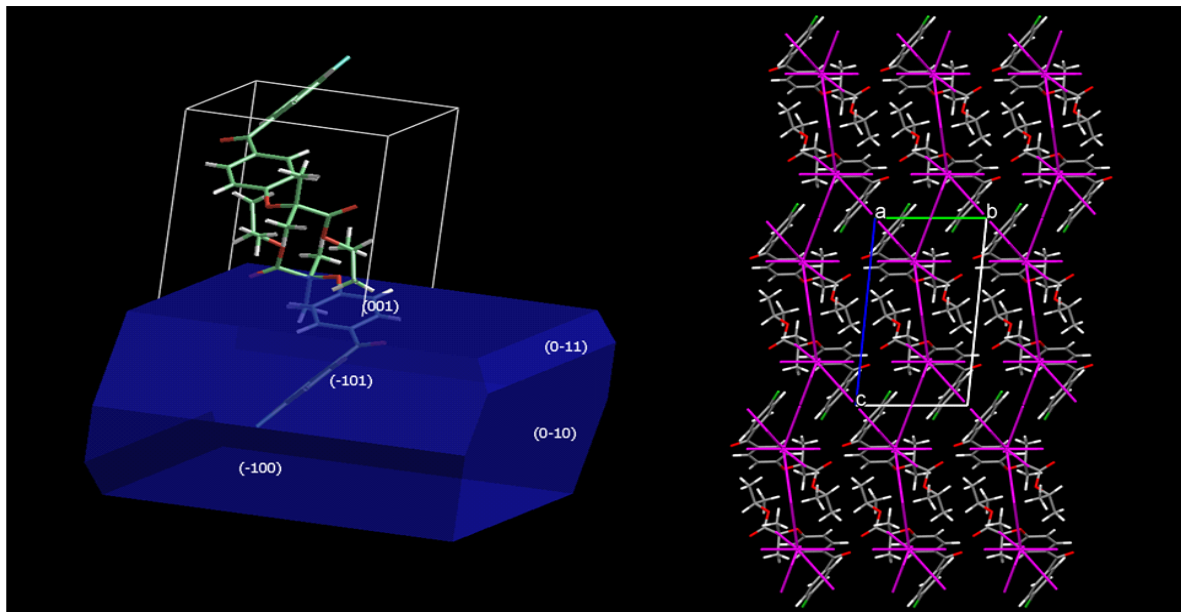


Figure 7. Crystal morphology and distribution of interaction forces in the crystal lattice of fenofibrate (projection along the crystallographic a axis).

3.4. Statistical Analysis of DoE Results

The process parameter and formulation factor effects considered in the experimental design, on the particle size distribution of the redispersed Fenofibrate suspensions, were analyzed statistically and the results are listed in Table 5 and presented graphically as 3-dimensional orthogonal plots in Figure 8a–c.

Table 5. Analysis of variance presenting the effects of variables A: Fenofibrate to stabilizer ratio (DSR), B: Fenofibrate to diluent ratio (DDR), C: operating inlet temperature (T), on the particle hydrodynamic diameter upon redispersion.

| Source | Sum of Squares | df | Mean Square | F-Value | <i>p</i> -Value |
|-----------|--------------------|----|--------------------|---------|-----------------|
| Model | 3.40×10^8 | 6 | 5.66×10^7 | 9.86 | 0.0007 |
| A-DSR | 9.87×10^7 | 1 | 9.87×10^7 | 17.19 | 0.0016 |
| B-DDR | 3.12×10^6 | 1 | 3.12×10^6 | 0.5424 | 0.4769 |
| C-T | 1.34×10^8 | 1 | 1.34×10^8 | 23.41 | 0.0005 |
| AB | 2.44×10^6 | 1 | 2.44×10^6 | 0.4251 | 0.5278 |
| AC | 1.06×10^8 | 1 | 1.06×10^8 | 18.42 | 0.0013 |
| BC | 3.83×10^6 | 1 | 3.83×10^6 | 0.6672 | 0.4314 |
| Residual | 6.32×10^7 | 11 | 5.74×10^6 | | |
| Cor Total | 4.03×10^8 | 17 | | | |

ANOVA of the results revealed the statistically significant factors (*p*-values < 0.05). The analysis suggests that the proposed model is significant, assigning an extremely limited probability of 0.07% that the results can be attributed to noise. The predicted R^2 value 0.5770 is in agreement to the adjusted R^2 of 0.7576 hence the difference appears less than 2 units of base. The signal to noise ratio > 4 is satisfactory in this case, confirming that the model allows us to explore the defined PQA design space.

The spray drying temperature exerts a significant linear effect on the particle size of the redispersed suspensions (*p*-value 0.0005; Figure 8b). The Fenofibrate to mannitol ratio does not affect the size of the final dried product within the investigated design space, as demonstrated by the contours of Figure 8a,c. In addition, the effect of the drug to stabilizer ratio is significant with a *p*-value of 0.0016, indicating that the reduction of Pharmacoat concentration relative to the drug results in an increase of the average particle size of the

dried Fenofibrate composition, as illustrated in Figure 8a,b. Finally, increase of inlet spray drying temperature translates to increased particle size of the reconstituted suspension.

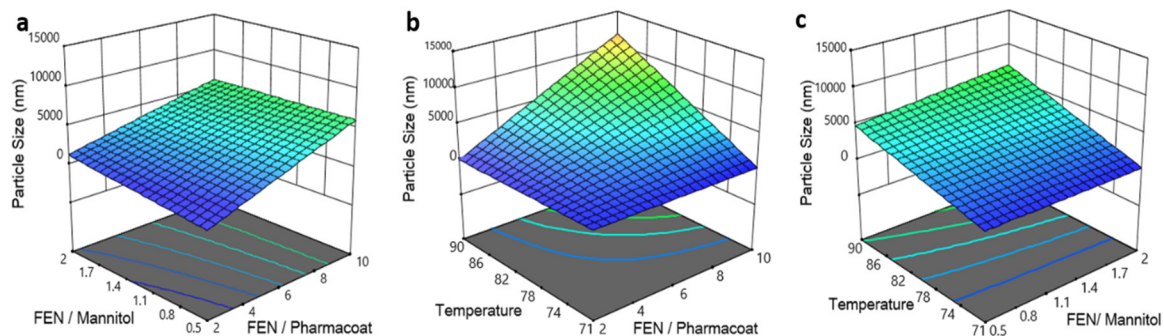


Figure 8. Response surface and contour plots of the particle size versus: (a) drug–diluent and drug–stabilizer ratio, (b) inlet temperature and drug–stabilizer ratio, (c) operating temperature and drug–mannitol ratio.

Table 6 lists the estimated coefficients for each term of the obtained model, which define the response per each unit of factorial change, when the remaining variables are held constant. The intercept refers to the average response overall and to the coefficients, thus imitating the calculated adjustments around the average based on the factor settings, the latter being considered orthogonal when VIFs approximate the value of 1. Elaborating on the former statement the variance inflation factor (VIF) refers to the model variance quotient with multiple terms, by the variance of one term alone. Therefore, VIF quantifies the multicollinearity severity in least squares regression analysis, providing a useful index of the quantity of the variance that a regression coefficient has increased due to collinearity [31].

Table 6. Coefficient estimates of the model for the response per each unit of factorial change, when the remaining variables are constant.

| Factor | Coefficient Estimates | df | Standard Error | 95% CI Low | 95% CI High | VIF |
|-----------|-----------------------|----|----------------|------------|-------------|------|
| Intercept | 3137.16 | 1 | 570.61 | 1881.26 | 4393.06 | |
| A—DSR | 2886.48 | 1 | 696.14 | 1354.29 | 4418.66 | 1.02 |
| B—DDR | 500.94 | 1 | 680.21 | −996.2 | 1998.07 | 1 |
| C—T | 2760.77 | 1 | 570.6 | 1504.9 | 4016.65 | 1.02 |
| AB | −541.06 | 1 | 829.85 | −2367.55 | 1285.42 | 1.02 |
| AC | 2961.58 | 1 | 690 | 1442.89 | 4480.26 | 1 |
| BC | 554.87 | 1 | 679.33 | −940.32 | 2050.07 | 1.02 |

The combined effect of increase of Fenofibrate and/or reduction of Pharmacoat concentration coupled with a temperature rise, results in a two-factor interaction coefficient of 2961.58 and a VF = 1. This behavior surpasses the negative size response owed to the reduction of the mannitol effect (see also AB interaction of estimated value of −541.06). The selected CQA optimization criteria regarding the Z-Average size response, taking into consideration the interactions between variables (Factor A) Fenofibrate to Pharmacoat ratio, (Factor B) Fenofibrate to mannitol ratio and operational inlet temperature (Factor C), are represented by the red solid dots commuting through the destination ramps of Figure 9a–d.

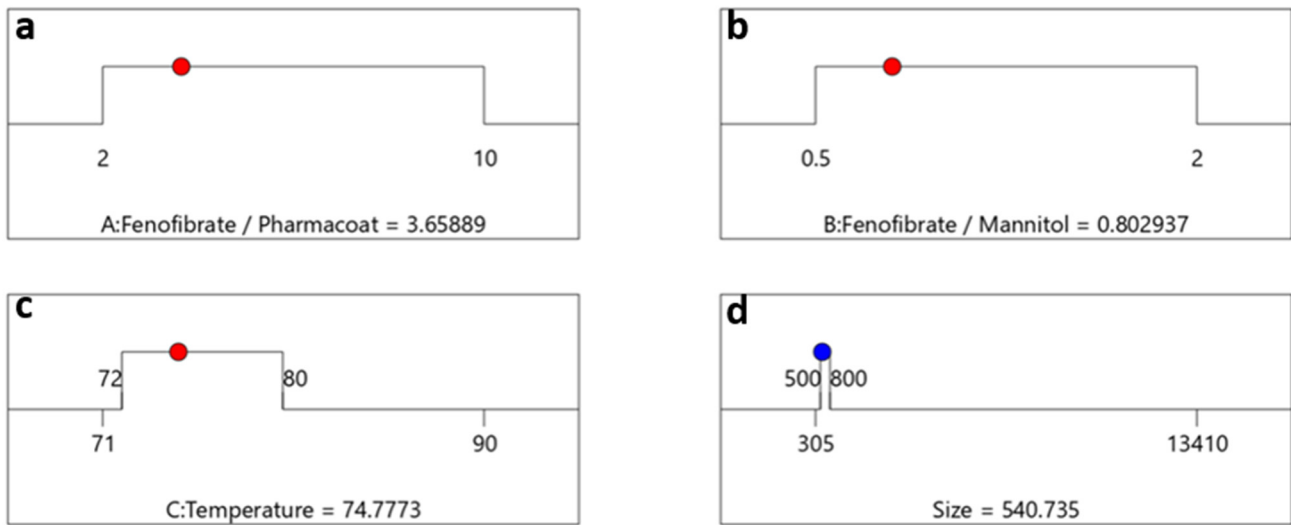


Figure 9. Optimization algebraic ramps outlining the solution meeting the criteria of desired CQAs. The factor settings of (a) drug–stabilizer, (b) drug–mannitol ratios, (c) inlet temperature, are shown by the red dots and (d) the CQA selected response prediction particle size values are displayed in blue.

The optimum factorial values demonstrated by the schematic railway representations of Figure 9a–c depict that formulating a Fenofibrate weight content of 3.65 times larger than Pharmacoat and 0.8 times less than mannitol, via spray drying performed at steady inlet temperature conditions of 75 °C, will most probably deliver a desired CQA of 540 nm particle diameter. In Figure 10, the contours of particle size distribution spanning the design mixture space i.e., Fenofibrate to diluent versus Fenofibrate to stabilizer ratio and the temperature factorial levels versus the above iterated mixture compositions are presented, achieving excellent values of desirability. The highlighted regions of interest are marked by the ellipse, while the red region depicts the most heavily populated area probable to meet the critical attributes of our DoE implemented in the Euclidian space.

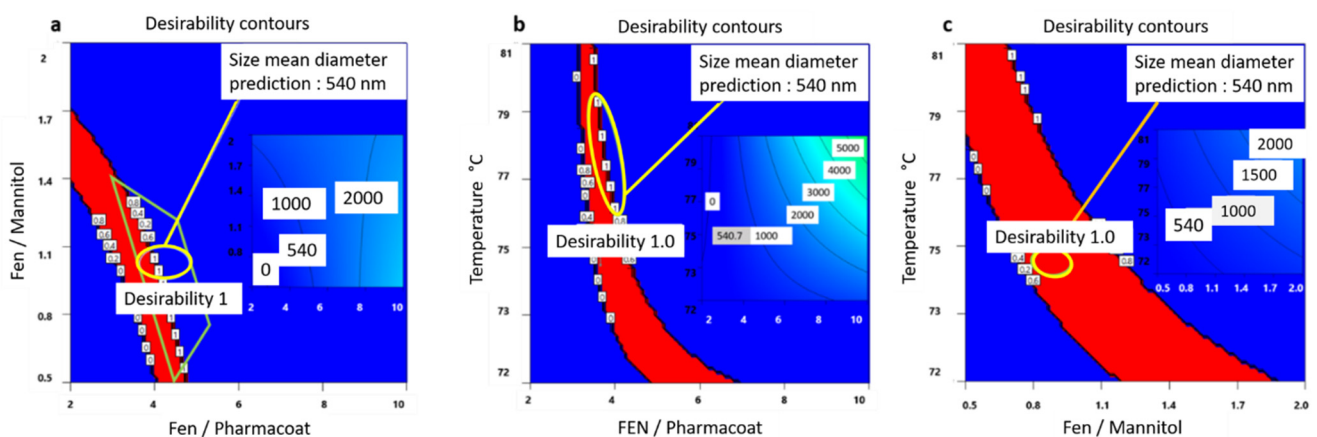


Figure 10. Desirability contours exploring the factorial space of: (a) Fenofibrate to mannitol and Fenofibrate to Pharmacoat w/w ratios, (b) inlet spray drying temperature and Fenofibrate to Pharmacoat w/w ratio, and (c) inlet spray drying temperature and Fenofibrate to mannitol w/w ratio. For each graph the optimum mean diameter prediction of 540.7 nm is flagged. Red contours direct the most heavily populated operational route of CQA of interest. For each graph the optimum desirability level is flagged. The inner rectangular shades show the variance of size of median diameter in the design space area.

Regarding the variability effects on the ζ -potential, the ANOVA results listed in Table 7 reveal that the proposed model is statistically significant, with only a 0.86% chance that the F-value would occur due to noise. The source of variance was further calculated for the

main effects and two-factor interactions. The main effects of Fenofibrate to stabilizer ratio (p -level 0.0029) and inlet temperature (p -level 0.0212) and the two-factor interaction between inlet temperature and Fenofibrate to mannitol ratio (p -level 0.0088), are the dominant factorial variables influencing the ζ -potential.

Table 7. Analysis of variance for the statistical significance of the investigated factors A: drug–stabilizer ratio (DSR), B: drug–mannitol ratio (DDR), C: inlet temperature (T), on the ζ -potential.

| Source | Sum of Squares | df | Mean Square | F-Value | p -Value |
|-----------|----------------|----|-------------|---------|------------|
| Model | 90.88 | 6 | 15.15 | 5.28 | 0.0086 |
| A-DSR | 41.4 | 1 | 41.4 | 14.44 | 0.0029 |
| B-DDR | 0.078 | 1 | 0.078 | 0.0272 | 0.872 |
| C-T | 20.67 | 1 | 20.67 | 7.21 | 0.0212 |
| AB | 1.99 | 1 | 1.99 | 0.6935 | 0.4227 |
| AC | 0.0958 | 1 | 0.0958 | 0.0334 | 0.8583 |
| BC | 29.01 | 1 | 29.01 | 10.12 | 0.0088 |
| Residual | 31.54 | 11 | 2.87 | | |
| Cor Total | 122.43 | 17 | | | |

Counterintuitively, and as shown by the plots of Figure 11a–c, it appears feasible within the boundaries of the given mixture contents and referring to the lab scale production settings, to pursue high Fenofibrate drug to excipient ratios, i.e., drug loading and low operating spray drying temperatures, without compromising the nanosuspensions' stability features. The predicted relationships for the ζ -potential were further assessed and the calculated model coefficient estimates, which represent the expected variance in response per unit change for each factor values when all the remaining factors are held constant, are shown in Table 8.

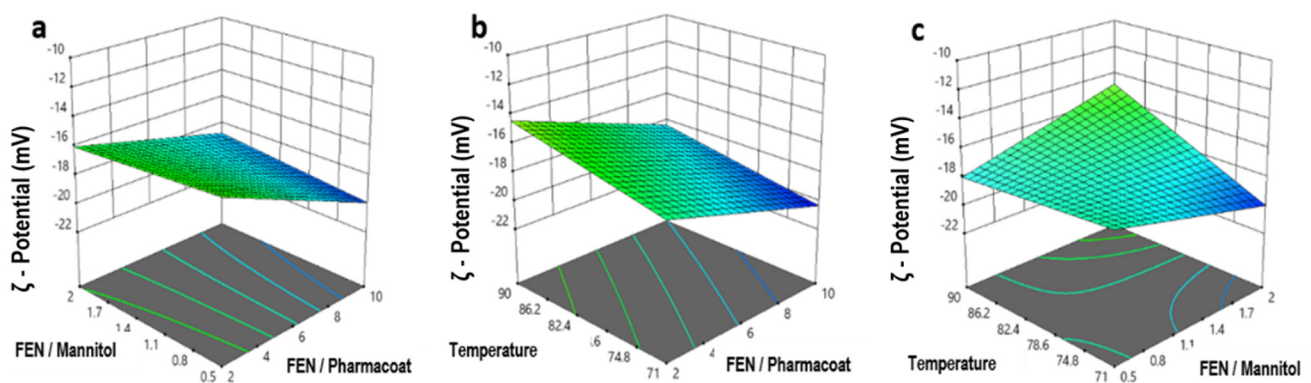


Figure 11. Response surface and contour plots of the ζ -potential versus: (a) drug–diluent and drug–stabilizer ratio, (b) inlet temperature and drug–stabilizer ratio, (c) operating temperature and drug–mannitol ratio.

The coefficient estimates represent the anticipated difference whereas the VIFs greater than unity indicate multicollinearity, i.e., the higher the VIF prediction the more severe the expected correlation of the factors, while in general VIF values of less than 10 are considered tolerable [31].

Table 8. Coefficient estimates demonstrating the response change per unit change in factor value when the remaining factors remain constant. The intercept is the average response of the runs while the coefficients are normalized by the average. For orthogonal factors the VIFs are 1; VIFs > 1 are indication of multicollinearity.

| Factor | Coefficient Estimate | df | Standard Error | 95% CI Low | 95% CI High | VIF |
|-----------|----------------------|----|----------------|------------|-------------|------|
| Intercept | −11.57 | 1 | 0.3766 | −12.40 | −10.74 | |
| A | 0.9689 | 1 | 0.4595 | −0.0424 | 1.98 | 1.02 |
| B | 0.9543 | 1 | 0.4490 | −0.0339 | 1.94 | 1.00 |
| C | 0.3957 | 1 | 0.3766 | −0.4332 | 1.22 | 1.02 |
| AB | −0.6684 | 1 | 0.5477 | −1.87 | 0.5371 | 1.02 |
| AC | 0.4974 | 1 | 0.4554 | −0.5050 | 1.50 | 1.00 |
| BC | −1.12 | 1 | 0.4484 | −2.11 | −0.1381 | 1.02 |

Expanding on this and as demonstrated by the response surface plot of Figure 11c, the decrease of temperature is correlated to the coefficient absolute value estimation of 0.3957 which in turn appears decisively responsible for the ζ -potential absolute value increase, stabilizing the nanosuspension. Our experimental findings also fall in line with first principle studies of calculating heat and mass balances, showing that the temperature is inversely proportional to the feed rate and proportional to the heated gas temperature [32]. Elaborating on the previous conclusion, the dryer's temperature and feed rate are defining the particle temperature and morphology which in turn affect the crystallization of the mixture droplets [33]. In this case the lab scale equipment with an air flow rate of 800 m³/h and a thin standard nozzle 0.7 mm favors the formation of younger droplets. This phenomenon directs either a discrete temperature rate increase of the particles or the boost of the aqueous solvent medium evaporation, hence both processes become more efficient and homogeneous in that fashion, while requiring a lower thermal input [34].

Having understood the material system's composition variables that might enhance stability, we then moved forward to set the CQA optimization criteria as represented by the destination ramps of Figure 12 for the ζ -potential of −16.7 mV, taking into account once more the interactions between drug–stabilizer ratio (Factor A), drug–mannitol ratio (Factor B) and inlet temperature (Factor C).

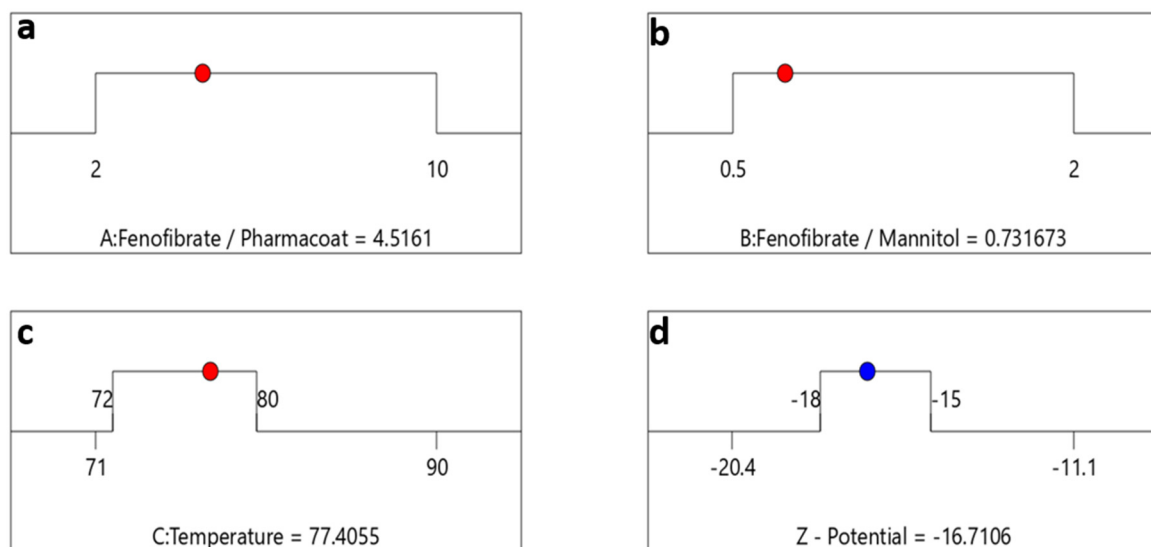


Figure 12. Optimization algebraic ramps outlining the optimal solution meeting the criteria of desired PQAs. The factor settings of (a) drug–stabilizer, (b) drug–mannitol ratios, (c) inlet temperature are shown by the red dots and (d) the CQA selected response prediction for ζ -potential values are displayed in blue.

The obtained overlay surface areas plotted by the yellow indication for the response range of the ζ -potential between the desired values -18 and -15 mV against the process parameters of temperature and the formulation composite factors of Fenofibrate/mannitol and Fenofibrate/Pharmacoat ratios, respectively, are illustrated in Figure 13. The diagram Figure 13c on the right is showing the optimum design space for the formulation of the API and the excipient contents of Pharmacoat and mannitol.

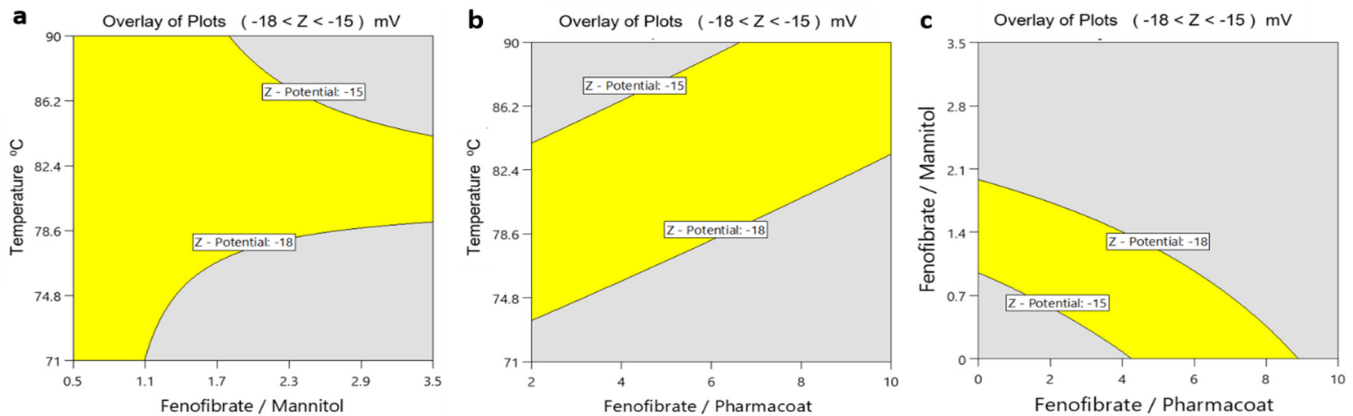


Figure 13. Overlay plots of ζ -potential: (a) inlet temperature and drug–mannitol ratio, (b) inlet temperature and drug–stabilizer ratio, (c) drug–mannitol and drug–stabilizer ratio.

According to Figure 13a,c, higher mannitol content clearly appears to contribute to higher stability of the nanosuspensions. Our experimental findings are in agreement with Maas and colleagues [35] who were able to prove that different states of spray dried mannitol particle surface topography may be acquired by crystallization processes that are diverse in speed. Lower temperatures crystallize mannitol-based materials to fine needles, forming acicular crystals that assemble in space as spheres with smooth surfaces. In contrast, according to the same study when the drying of such materials is performed at high temperatures, then the acclaimed high evaporation rate poses inverse impact on the nucleation event. This phenomenon roots the formation of a metastable, supersaturated and viscous liquid which finally crystallizes to spheres of coarse surfaces triggered by a second nucleation occurrence [35], which in turn may affect the stabilizer surface adsorption. Importantly the iterated surface roughness results in lower absolute ζ -potential values, an assumption absolutely consistent with our experimental findings [36].

Design Space Optimization for the Lab Scale Production of Fenofibrate Nanocrystals

Combining the insights gained by the optimization of both the experimentally investigated processes, we can proceed with the attempt to define “universal” CQA optimization criteria. The latter consist of the combinatory selected responses, namely the Z-Average size and the ζ -potential investigated through the various interactions of factorial variables i.e., drug–stabilizer ratio (Factor A), drug–mannitol ratio (Factor B) and inlet temperature (Factor C), represented herein by the lines of the destination ramps of Figure 14a–c, incorporating the process drying temperatures above and below the API’s homologous melting point to our design space.

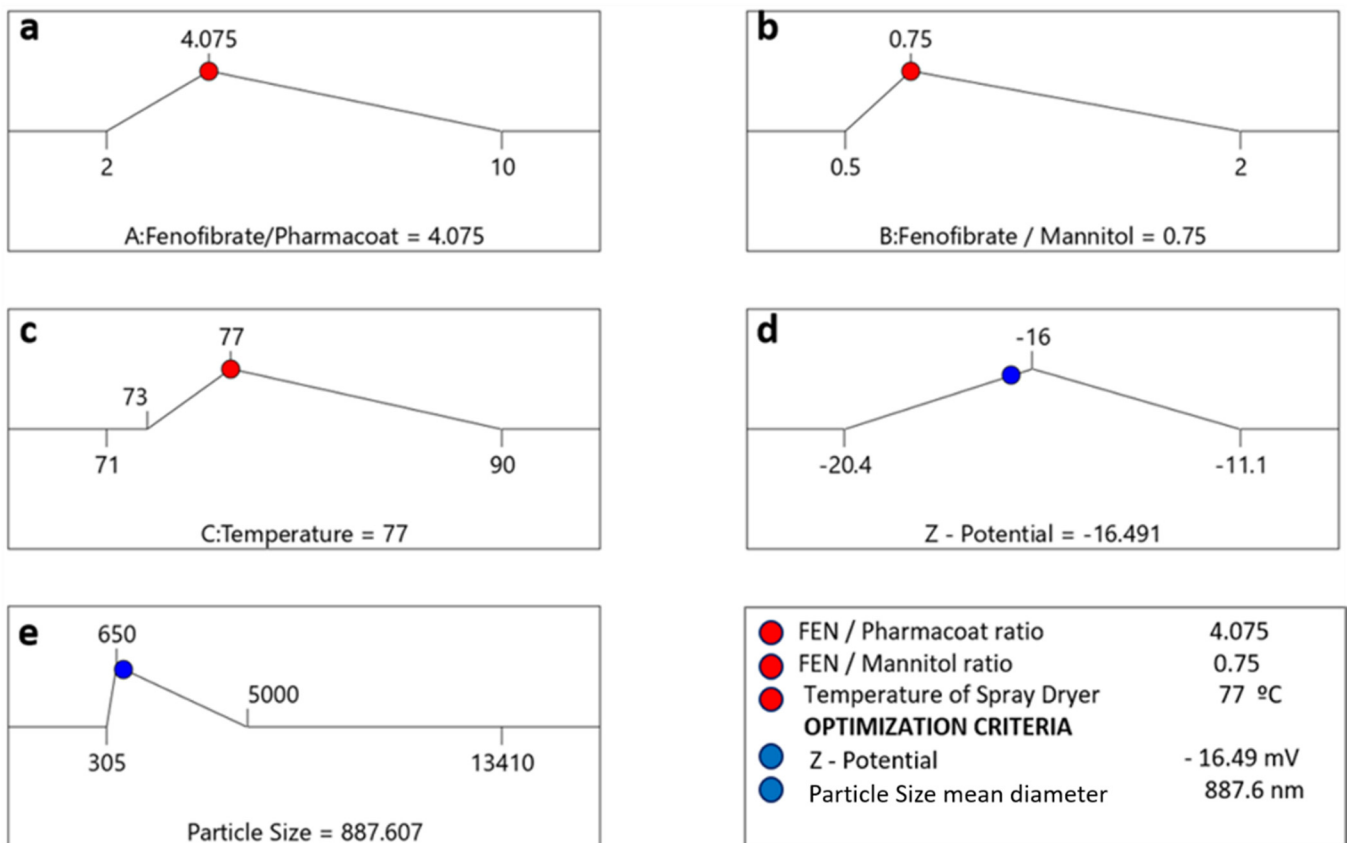


Figure 14. Numeric optimization ramps investigating the optimal solution meeting the criteria of the desired CQAs (right lower corner blue circle indications). The optimal factor settings of inlet temperature, drug–stabilizer and drug–mannitol ratios are shown with red dots, while the optimal response prediction values are displayed in blue: (a) average particle size was set at 887.6 nm; (b) algebraic ζ -potential corresponding at -16.49 mV and set inlet temperature 77 °C (c) temperature corresponding at -16.49 mV and set inlet temperature 77 °C (d) ζ -potential outlier values (e) particle size outlier values.

The obtained QbD operational space showing the controlled variables that conform to the desired CQA criteria for the total unit block operations are displayed by the clustered Figure 15a–c. Having analyzed the multivariable system, an overall complementarity proposed solution of excellent desirability projected value of 0.966 for DSR and DDR, HT and DSR, HT and DDR, guides the configuration of the optimum nanosuspension mixture specifications and those of the operating inlet spray drying temperature conditions.

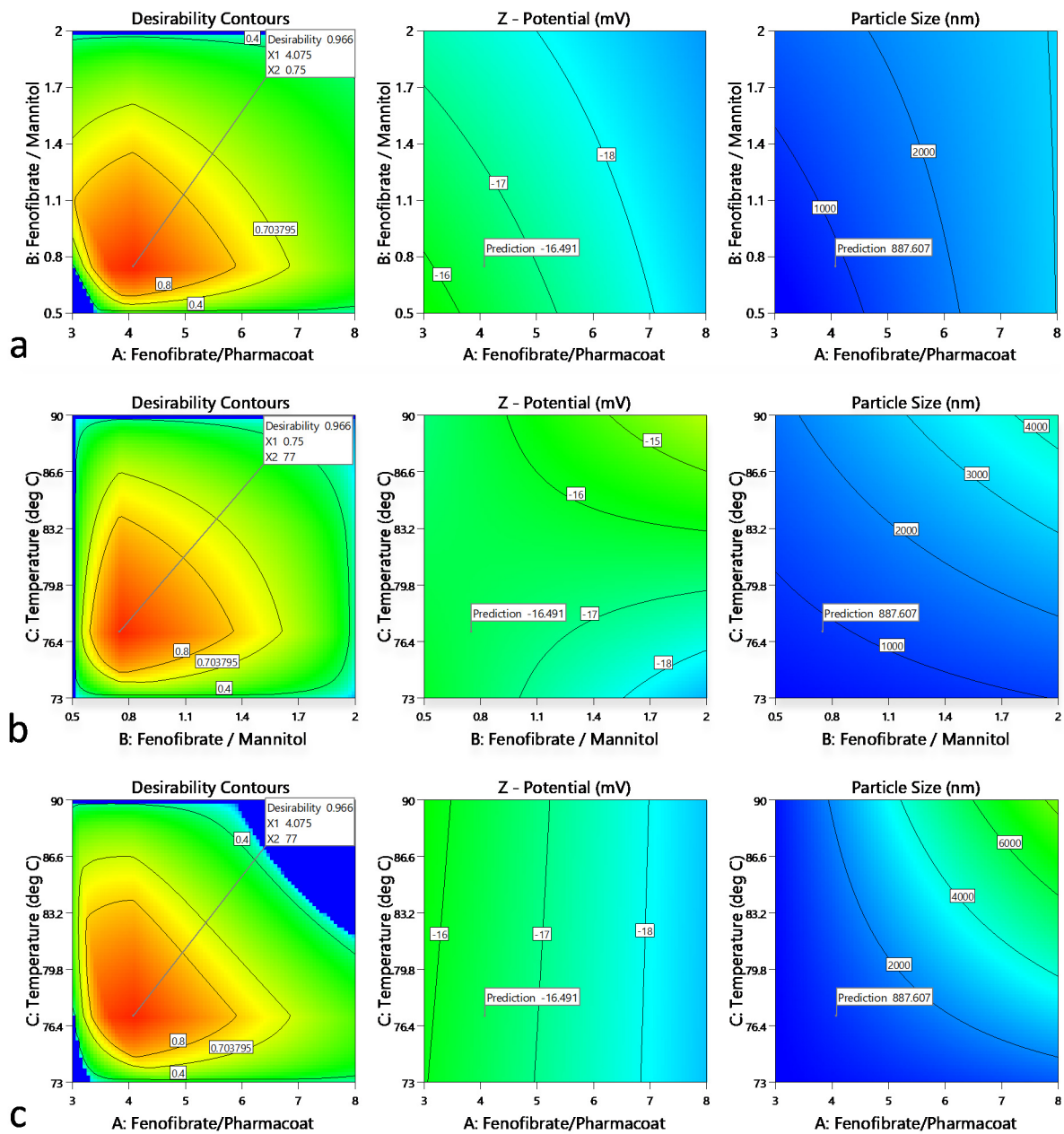


Figure 15. Contour overall plots are presented showing the desirability as function of factorial functions guiding the exploration of the design interaction space: (a) Fenofibrate to Pharmacoat and Fenofibrate to mannitol w/w ratios, (b) Fenofibrate to mannitol w/w ratio and inlet temperature, (c) Fenofibrate to Pharmacoat w/w ratio and inlet temperature. For each graph on the left column the optimum of ζ -potential and Z-size responses are flagged in the medium and the left column, respectively. Inner red to perimeter blue face contours define the operational CQA area of interest.

4. Conclusions

The effects of formulation variables and process parameters governing ball milling comminution coupled with spray drying of Fenofibrate nanosuspensions at temperatures approaching melting point were investigated. The resolved operating conditions supported by experimental and theoretical approaches, suggest that API submicron crystals of approximately 887 nm of average hydrodynamic diameter, bearing the ζ -potential of -16.49 mV, are efficiently obtained employing the Fenofibrate to Pharmacoat/mannitol weighted optimum ratios of 4.075% and 0.75%, respectively, dried at the preferred temperature of 77 °C. Reduction of particle API size below the 1 μm will generate nanocrystals, improving both drug solubility and bioavailability [37]. Therefore, the rationalization of

the formulated material's behavior via the proposed QbD methodology assisted by theoretical calculations minimizes the risk of temperature-related degradation of uniformity, at the same time reducing development costs by narrowing the focus of the operational space. The method can be further applied to enable the manipulation or fine tuning of compositions incorporating thermolabile or even prone to eutectic formation APIs, under increased quality assurance.

Author Contributions: Conceptualization, K.K. and A.O.; methodology, A.O. and K.K.; software, K.K. and A.O.; validation, A.O. and K.K.; formal analysis, C.M. and A.O.; investigation, N.G., K.K., A.O.; resources, I.N. and A.O.; data curation, N.G. and A.O.; writing—review and editing, N.G., A.O. and K.K.; visualization, N.G., A.O. and K.K.; supervision, K.K.; project administration, K.K.; funding acquisition, not applicable. All authors have read and agreed to the published version of the manuscript.

Funding: This research received no external funding.

Institutional Review Board Statement: Not applicable.

Informed Consent Statement: Not applicable.

Data Availability Statement: Not applicable.

Conflicts of Interest: The authors declare no conflict of interest.

References

1. Ling, H.; Luoma, J.T.; Hilleman, D. A Review of Currently Available Fenofibrate and Fenofibric Acid Formulations. *Cardiol. Res.* **2013**, *4*, 47–55. [[CrossRef](#)]
2. Back, H.M.; Song, B.; Pradhan, S.; Chae, J.W.; Han, N.; Kang, W.; Chang, M.J.; Zheng, J.; Kwon, K.I.; Karlsson, M.O.; et al. A mechanism-based pharmacokinetic model of fenofibrate for explaining increased drug absorption after food consumption. *BMC Pharmacol. Toxicol.* **2018**, *19*, 4. [[CrossRef](#)]
3. Noyes, A.A.; Whitney, W.R. The rate of solution of solid substances in their own solutions. *J. Am. Chem. Soc.* **1897**, *19*, 930–934. [[CrossRef](#)]
4. Ghosh, I.; Schenck, D.; Bose, S.; Ruegger, C. Optimization of formulation and process parameters for the production of nanosuspension by wet media milling technique: Effect of Vitamin E TPGS and nanocrystal particle size on oral absorption. *Eur. J. Pharm. Sci.* **2012**, *47*, 718–728. [[CrossRef](#)] [[PubMed](#)]
5. Dudognon, E.; Willart, J.F.; Caron, V.; Capet, F.; Larsson, T.; Descamps, M. Formation of budesonide/ α -lactose glass solutions by ball-milling. *Solid State Commun.* **2006**, *138*, 68–71. [[CrossRef](#)]
6. Branham, M.L.; Moyo, T.; Govender, T. Preparation and solid-state characterization of ball milled saquinavir mesylate for solubility enhancement. *Eur. J. Pharm. Biopharm.* **2012**, *80*, 194–202. [[CrossRef](#)] [[PubMed](#)]
7. Eskin, D.; Zhupanska, O.; Hamey, R.; Moudgil, B.; Scarlett, B. Microhydrodynamics of stirred media milling. *Powder Technol.* **2005**, *156*, 95–102. [[CrossRef](#)]
8. Lu, G.; Duan, Y.-Y.; Wang, X.-D. Surface tension, viscosity, and rheology of water-based nanofluids: A microscopic interpretation on the molecular level. *J. Nanopart. Res.* **2014**, *16*, 2564. [[CrossRef](#)]
9. Peltonen, L.; Hirvonen, J. Pharmaceutical nanocrystals by nanomilling: Critical process parameters, particle fracturing and stabilization methods. *J. Pharm. Pharmacol.* **2010**, *62*, 1569–1579. [[CrossRef](#)] [[PubMed](#)]
10. Malkin, A.I. Regularities and mechanisms of the Reh binder's effect. *Colloid J.* **2012**, *74*, 223–238. [[CrossRef](#)]
11. Arpagaus, C. Pharmaceutical Particle Engineering via Nano Spray Drying—Process Parameters and Application Examples on the Laboratory-Scale. *Int. J. Med. Nano Res.* **2018**, *5*. [[CrossRef](#)]
12. Górnjak, A.; Wojakowska, A.; Karolewicz, B.; Pluta, J. Phase diagram and dissolution studies of the fenofibrate-acetylsalicylic acid system. *J. Therm. Anal. Calorim.* **2011**, *104*, 1195–1200. [[CrossRef](#)]
13. Zuo, B.; Sun, Y.; Li, H.; Liu, X.; Zhai, Y.; Sun, J.; He, Z. Preparation and in vitro/in vivo evaluation of fenofibrate nanocrystals. *Int. J. Pharm.* **2013**, *455*, 267–275. [[CrossRef](#)] [[PubMed](#)]
14. Van Eerdenbrugh, B.; Froyen, L.; Van Humbeeck, J.; Martens, J.A.; Augustijns, P.; Van den Mooter, G. Drying of crystalline drug nanosuspensions—The importance of surface hydrophobicity on dissolution behavior upon redispersion. *Eur. J. Pharm. Sci.* **2008**, *35*, 127–135. [[CrossRef](#)] [[PubMed](#)]
15. Xia, D.; Shrestha, N.; van de Streek, J.; Mu, H.; Yang, M. Spray drying of fenofibrate loaded nanostructured lipid carriers. *Asian J. Pharm. Sci.* **2016**, *11*, 507–515. [[CrossRef](#)]
16. Vogt, M.; Kunath, K.; Dressman, J.B. Dissolution enhancement of fenofibrate by micronization, cogrinding and spray-drying: Comparison with commercial preparations. *Eur. J. Pharm. Biopharm.* **2008**, *68*, 283–288. [[CrossRef](#)]
17. Yue, P.F.; Li, Y.; Wan, J.; Yang, M.; Zhu, W.F.; Wang, C.H. Study on formability of solid nanosuspensions during nanodispersion and solidification: I. Novel role of stabilizer/drug property. *Int. J. Pharm.* **2013**, *454*, 269–277. [[CrossRef](#)]

18. Rissanou, A.N.; Ouranidis, A.; Karatasos, K. Complexation of single stranded RNA with an ionizable lipid: An all-atom molecular dynamics simulation study. *Soft Matter* **2020**, *16*, 6993–7005. [[CrossRef](#)]
19. Gavezzotti, A. Calculations of lattice energies of organic crystals: The PIXEL integration method in comparison with more traditional methods. *Z. Krist.* **2005**, *220*, 499–510. [[CrossRef](#)]
20. Groom, C.R.; Bruno, I.J.; Lightfoot, M.P.; Ward, S.C. The Cambridge Structural Database. *Acta Crystallogr. Sect. B Struct. Sci.* **2016**, *72*, 171–179. [[CrossRef](#)]
21. Fleming, S.; Rohl, A. GDIS: A visualization program for molecular and periodic systems. *Zeitschrift fur Krist.* **2005**, *220*, 580–584. [[CrossRef](#)]
22. Gale, J.D.; Rohl, A.L. The General Utility Lattice Program (GULP). *Mol. Simul.* **2003**, *29*, 291–341. [[CrossRef](#)]
23. Mayo, S.L.; Olafson, B.D.; Goddard, W.A. DREIDING: A Generic Force Field for Molecular Simulations. *J. Phys. Chem.* **1990**, *94*, 8897–8909. [[CrossRef](#)]
24. Schmidt, M.W.; Baldridge, K.K.; Boatz, J.A.; Elbert, S.T.; Gordon, M.S.; Jensen, J.H.; Koseki, S.; Matsunaga, N.; Nguyen, K.A.; Su, S.; et al. General atomic and molecular electronic structure system. *J. Comput. Chem.* **1993**, *14*, 1347–1363. [[CrossRef](#)]
25. Shishkin, O.; Medvediev, V.; Zubatyuk, R. Supramolecular architecture of molecular crystals possessing shearing mechanical properties: Columns versus layers. *CrystEngComm* **2012**, *15*, 160–167. [[CrossRef](#)]
26. Bond, A.D. processPIXEL: A program to generate energy-vector models from Gavezzotti's PIXEL calculations. *J. Appl. Crystallogr.* **2014**, *47*, 1777–1780. [[CrossRef](#)]
27. Macrae, C.F.; Edgington, P.R.; McCabe, P.; Pidcock, E.; Shields, G.P.; Taylor, R.; Towler, M.; Van De Streek, J. Mercury: Visualization and analysis of crystal structures. *J. Appl. Crystallogr.* **2006**, *39*, 453–457. [[CrossRef](#)]
28. Singh, A.; Van den Mooter, G. Spray drying formulation of amorphous solid dispersions. *Adv. Drug Deliv. Rev.* **2016**, *100*, 27–50. [[CrossRef](#)]
29. Tipduangta, P.; Takeddin, K.; Fábán, L.; Belton, P.; Qi, S. A new low melting-point polymorph of fenofibrate prepared via talc induced heterogeneous nucleation. *Cryst. Growth Des.* **2015**, *15*, 5011–5020. [[CrossRef](#)]
30. Ferjani, H. Structural, Hirshfeld Surface Analysis, Morphological Approach, and Spectroscopic Study of New Hybrid Iodobismuthate Containing Tetranuclear 0D Cluster $\text{Bi}_4\text{I}_{16}\cdot 4(\text{C}_6\text{H}_9\text{N}_2)_2(\text{H}_2\text{O})$. *Crystals* **2020**, *10*, 397. [[CrossRef](#)]
31. Marquardt, D.W. Generalized inverses, ridge regression, biased linear estimation, and nonlinear estimation. *Technometrics* **1970**, *12*, 591–612. [[CrossRef](#)]
32. Ouranidis, A.; Gkampelis, N.; Vardaka, E.; Karagianni, A.; Tsiptsios, D.; Nikolakakis, I.; Kachrimanis, K. Overcoming the solubility barrier of ibuprofen by the rational process design of a nanocrystal formulation. *Pharmaceutics* **2020**, *12*, 969. [[CrossRef](#)]
33. Longest, P.W.; Farkas, D.; Hassan, A.; Hindle, M. Computational Fluid Dynamics (CFD) Simulations of Spray Drying: Linking Drying Parameters with Experimental Aerosolization Performance. *Pharm. Res.* **2020**, *37*, 101. [[CrossRef](#)]
34. Littringer, E.M.; Mescher, A.; Eckhard, S.; Schröttner, H.; Langes, C.; Fries, M.; Griesser, U.; Walzel, P.; Urbanetz, N.A. Spray drying of Mannitol as a drug carrier—the impact of process parameters on product properties. *Dry. Technol.* **2012**, *30*, 114–124. [[CrossRef](#)]
35. Maas, S.G.; Schaldach, G.; Littringer, E.M.; Mescher, A.; Griesser, U.J.; Braun, D.E.; Walzel, P.E.; Urbanetz, N.A. The impact of spray drying outlet temperature on the particle morphology of mannitol. *Powder Technol.* **2011**, *213*, 27–35. [[CrossRef](#)]
36. Drechsler, A.; Caspari, A.; Synytska, A. Influence of roughness and capillary size on the zeta potential values obtained by streaming potential measurements. *Surf. Interface Anal.* **2020**, *52*, 991–995. [[CrossRef](#)]
37. Ouranidis, A.; Tsixerli, A.; Vardaka, E.; Markopoulou, C.K.; Zacharis, C.K.; Nicolaou, I.; Hatzichristou, D.; Haidich, A.-B.; Kostomitsopoulos, N.; Kachrimanis, K. Sildenafil 4.0—Integrated Synthetic Chemistry, Formulation and Analytical Strategies Effecting Immense Therapeutic and Societal Impact in the Fourth Industrial Era. *Pharmaceutics* **2021**, *14*, 365. [[CrossRef](#)]